MICROCOPY RESOLUTION TEST CHART
NATIONAL BUREAU OF STANDARDS-1963-A

Applications of Spectral Estimation Techniques to Radar Doppler Processing

Simulation and Analysis of HF Skywave Radar Data

DENNIS B. TRIZNA AND GEORGE D. MCNEAL

Radar Techniques Branch
Radar Division

December 31, 1985

NAVAL RESEARCH LABORATORY
Washington, D.C.

AD-A165 153

REPORT DOCUMENTATION PAGE

1a. REPORT SECURITY CLASSIFICATION	1b. RESTRICTIVE MARKINGS
UNCLASSIFIED	

2a. SECURITY CLASSIFICATION AUTHORITY	3. DISTRIBUTION / AVAILABILITY OF REPORT
	Approved for public release; distribution unlimited.
2b. DECLASSIFICATION / DOWNGRADING SCHEDULE	

4. PERFORMING ORGANIZATION REPORT NUMBER(S)	5. MONITORING ORGANIZATION REPORT NUMBER(S)
NRL Report 8950	

6a. NAME OF PERFORMING ORGANIZATION	6b. OFFICE SYMBOL (If applicable)	7a. NAME OF MONITORING ORGANIZATION
Naval Research Laboratory	5320	

6c. ADDRESS (City, State, and ZIP Code)	7b. ADDRESS (City, State, and ZIP Code)
Washington, DC 20375-5000	

8a. NAME OF FUNDING / SPONSORING ORGANIZATION	8b. OFFICE SYMBOL (If applicable)	9. PROCUREMENT INSTRUMENT IDENTIFICATION NUMBER
Naval Electronic Systems Command		

8c. ADDRESS (City, State, and ZIP Code)	10. SOURCE OF FUNDING NUMBERS			
	PROGRAM ELEMENT NO.	PROJECT NO.	TASK NO.	WORK UNIT ACCESSION NO.
Washington, DC 20360	62712N	XF12151		DN155-106

11. TITLE (Include Security Classification)

Applications of Spectral Estimation Techniques to Radar Doppler Processing:
Simulation and Analysis of HF Skywave Radar Data

12. PERSONAL AUTHOR(S)
Trizna, D.B. and McNeal, G.D.

13a. TYPE OF REPORT	13b. TIME COVERED	14. DATE OF REPORT (Year, Month, Day)	15. PAGE COUNT
Interim	FROM _____ TO _____	1985 December 31	31

16. SUPPLEMENTARY NOTATION

17.	COSATI CODES		18. SUBJECT TERMS (Continue on reverse if necessary and identify by block number)
FIELD	GROUP	SUB-GROUP	Radar detection Spectral estimation
			Doppler processing Radar clutter

19. ABSTRACT (Continue on reverse if necessary and identify by block number)

This work is the second paper in a series of studies of the application of spectral estimations techniques to Doppler processing of coherent radar signals. In this work, simulated high-frequency (HF) radar sea scatter time series are generated and processed by use of three different spectral estimation algorithms and the fast Fourier transform (FFT). The sea clutter is simulated by narrowband filtering a wideband Gaussian noise spectrum in the frequency domain, with filter widths appropriate to describe first-order Bragg lines and second-order continuum. Targets are introduced as sinusoids, stepped by 5 dB for eight different echo power values, and stepped in Doppler frequency for four different values relative to the clutter. These simulations identify problems that appear unique to Doppler processing of coherent radar data in the presence of broadband clutter, and are in distinction to the application of spectral estimation to processing in the spatial domain. In the latter case, the spectral contributions are generally narrowly confined in the angular power spectral estimate, and the aim is to separate these contributions in the presence of noise. The HF radar application is concerned with separation of weak targets in the presence of stronger clutter returns, which are relatively broad compared to the target return. It appears that the Burg maximum entropy method allows the detection of targets in clutter under conditions which the FFT is incapable of detection with any degree of certainty.

20. DISTRIBUTION / AVAILABILITY OF ABSTRACT	21. ABSTRACT SECURITY CLASSIFICATION
☐ UNCLASSIFIED/UNLIMITED ☒ SAME AS RPT. ☐ DTIC USERS	UNCLASSIFIED

22a. NAME OF RESPONSIBLE INDIVIDUAL	22b. TELEPHONE (Include Area Code)	22c. OFFICE SYMBOL
D.B. Trizna/G.D. McNeal	(202) 767-4873	5303.1/5320

DD FORM 1473, 84 MAR   83 APR edition may be used until exhausted.   SECURITY CLASSIFICATION OF THIS PAGE
All other editions are obsolete.

i

CONTENTS

Accesion For

NTIS CRA&I	☑
DTIC TAB	☐
U: announced	☐
Justification	

By ....

Distribution /

Availability Codes

Dist	Avail and / or Special
A-1	

iii

APPLICATIONS OF SPECTRAL ESTIMATION TECHNIQUES TO RADAR DOPPLER PROCESSING

SIMULATION AND ANALYSIS OF HF SKYWAVE RADAR DATA

INTRODUCTION

Spectral estimation is one useful application of autoregressive modeling by using data consisting of a finite series of amplitude samples of an analog signal in space or time. Other applications include robotic control and recursive digital filtering. The technique of autoregressive (AR) spectral estimation is based on developing a model for an infinite time series by using a finite set of data samples. Thus, higher spectral resolution is achieved by estimating power spectra from such a model than could be obtained by calculating the power spectra by use of traditional Fourier transform processing of the finite data record. Spectral estimation techniques have been applied in the field of radar primarily in the spatial/wave-number domain (see, for example, Gabriel [1], for a comprehensive review of this area). Samples collected over a few-element antenna array in space are used to identify the location of strong signals in the transform space (wave number or azimuthal angle), with much higher angular resolution than could be achieved with Fourier-transform processing.

Very little work has been done in the area of spectral estimation for Doppler processing of coherent radar data. The only work known to the authors has been a comparison of the Marple algorithm with fast fourier transform (FFT) processing of high-frequency (HF) radar data [2] for targets far from the clutter. Only a qualitative comparison of the two techniques was made, with no quantitative conclusions drawn. In some cases better results were observed by using a shorter number of data points for input into the spectral estimation algorithms than more, although Cooley [2] did not discuss the reason for this behavior. We have observed the same type of behavior in considering real data, and we will discuss the apparent reason for this behavior in a later paper in this series.

In the second section we present a simulation of an HF radar Doppler spectrum, including both targets and clutter. This is accomplished by generating a time series consisting of a sinusoidal signal to represent the target return. Two different methods are used to represent the sea clutter. The first uses two sinusoids to represent the first-order Bragg lines; the second represents them with a very narrow-band Gaussian profile. In both cases, second-order sea clutter is represented by broader band-limited noise in a similar manner. These narrowband noise signals are generated in the following way. A white-noise complex spectrum is operated on by a narrowband filter with a Gaussian profile. This is then inverse-transformed to the time domain to represent a component of the sea clutter. An independent time series is required to represent each component of the clutter, and these are summed along with the target sine wave and low-level unfiltered white noise, to represent the composite time series signal.

These simulated time-series data are processed by using traditional FFT techniques with long time records to show the "true" spectral characteristics. Then several AR spectral estimation algorithms are applied by using much shorter time records to demonstrate the high-resolution feature of spectral estimation techniques, i.e., the ability to achieve the same spectral resolution as FFT processing with far fewer points. Three different methods are compared: the Burg maximum entropy method, the covariance method, and the autocorrelation method.

CHARACTERISTICS OF THE HF RADAR SEA ECHO

Because of the relatively narrow bandwidths used at HF due to the crowded spectrum environment, relatively long pulse lengths result when compared to those for other radar frequencies. The clutter return that results for these long pulse lengths creates a situation in which the detection of targets is representative of a clutter-limited environment. The Doppler spectrum of sea scatter is sufficiently complex so that the application of traditional clutter cancellation techniques typically is not feasible when attempting to detect slow moving ships. Therefore, radar processing strategies require high dynamic range capabilities, in the order of 80 dB or more, so that the sea echo return may be processed in a coherent fashion and target returns may be distinguished in the Doppler spectrum.

Because of the high resolution required to separate slow moving targets from the clutter, relatively long coherent integration times are required. These are typically longer than might be desirable for effective illumination strategies which incorporate short coherent dwell times, either over several azimuthal positions or over several operating frequencies for extensive range coverage. Hence, the Doppler resolution advantages offered by spectral estimation techniques, typically ten times that of the FFT, make these techniques an attractive option for HF Doppler processing. However, very little work has been done in the area of detecting coherent sinusoids in the presence of a relatively broadband signal in the Doppler domain. The simulation presented in this section attempts to address this deficiency.

The radar echo from the sea at HF consists of first- and second-order contributions which can differ between 20 dB to more than 40 dB. This difference depends on radar aspect relative to primary wave direction and wave amplitude in the echoing area [3]. The first-order echo is due primarily to Bragg scatter, i.e., scatter from those ocean wave spectral components with wavelength L, satisfying:

$$L = \lambda/(2 \cos \phi), \tag{1}$$

where λ is the radar wavelength and ϕ is the grazing angle of the incident radar energy relative to the surface.

Because these Bragg-resonant ocean waves travel at a phase velocity that depends on their wavelength, and because the Bragg resonance is so narrowbanded a process, the Doppler resonant sea echo for line-of-sight illumination is quite narrow as well. For the case of skywave illumination via the ionosphere, propagation effects tend to broaden the Bragg lines in the Doppler spectrum compared to the line-of-sight values. (See Trizna [3] for a discussion of the limiting width of sea scatter Doppler spectral lines imposed by the ionosphere.) In addition, because of the broad radar wave front incident on the surface, only those components from the directional ocean wave spectrum which are traveling toward and away from the radar will coherently backscatter energy to the radar. Hence, for a radar frequency of f_R in megahertz, the radar echo from approaching and receding components will be shifted in Doppler frequency by an equal amount, df, either side of zero in hertz:

$$df = 2fv/c = 0.102(f_R)^{1/2}. \tag{2}$$

The dispersion rule for gravity ocean waves has been used to derive the second half of Eq. (2), along with Eq. (1) with

$$\phi = 0°.$$

This gravity wave dispersion rule is given by:

$$\Omega^2 = gK \tag{3}$$

where Ω is the ocean wave frequency and g is the acceleration of gravity.

2

Because of the narrowband nature of the scattering mechanism, the first-order radar returns in the Doppler spectrum can be modeled by a pair of nearly discrete returns in the spectrum, with relative amplitudes which differ from between 0 to 30 dB, depending on the radar-wind/wave aspect again. For cross-wind illumination, the two radar echoes are equal in amplitude, whereas for the upwind or downwind illumination, the difference is the maximum. The second-order spectrum is typically 20 to 40 dB less than the greatest first-order peak, with spectral structure appearing between the first-order lines as well as to either side of them [3]. The level of the second-order energy varies with aspect angle for fixed sea conditions, as well as with varying sea conditions for fixed aspect.

Figure 1 shows an example of a pair of such spectra collected in a line-of-sight propagation mode, for two different sea conditions, the higher seas represented on the left. The spectrum consists of two first-order Bragg lines, at $+-1$ in Doppler; the second-order continuum between the Bragg lines, ZETA db down from the strongest Bragg line; and second-order structure outside of the stronger Bragg line. Concerning this third region, we shall assume the structure to be relatively broad in Doppler in the simulation of its time series representation, as is observed in skywave propagation.
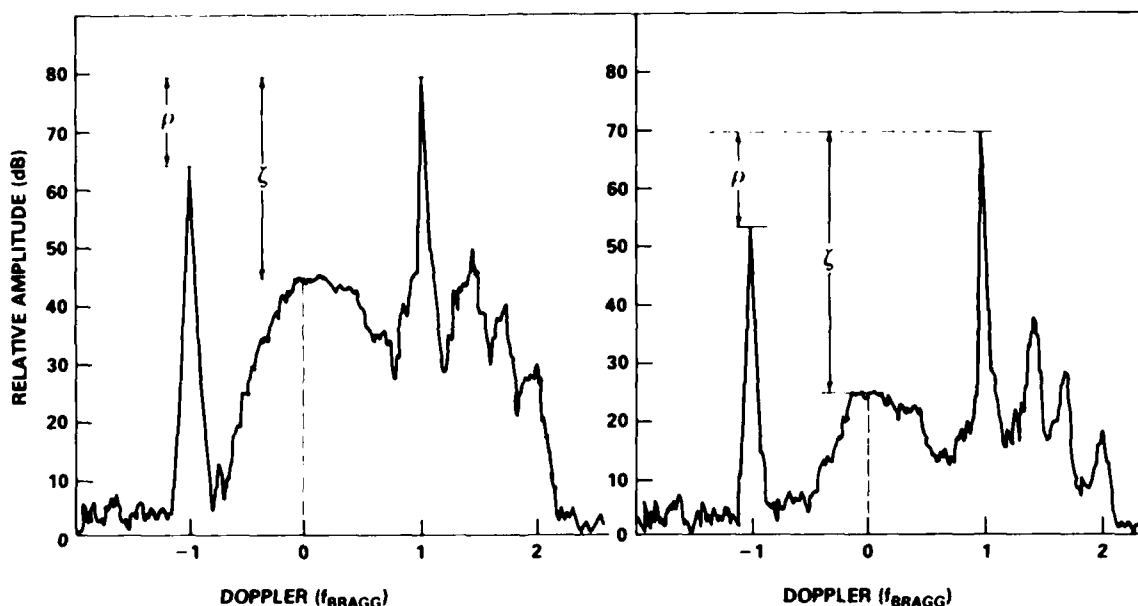

Fig. 1 — HF radar Doppler sea scatter spectra are shown for two different sea conditions and similar spread of wave energy in angle about the wind. The spectra were normalized in Doppler frequency by dividing by the Bragg frequency given in Eq. (2). First-order Bragg lines described in the text occur at ± 1 in Doppler frequency, while the lower level second-order structure lies at much lower level amplitudes.

SIMULATION OF THE FIRST- AND SECOND-ORDER HF SEA ECHO

In the following treatment we have modeled the first- and second-order sea echo by two different methods, both of which consider the second-order scatter as narrowband Gaussian processes. In the first method, the first-order Bragg lines were modeled as sinusoids, resulting in spectral line widths determined only by the length of the data record input into the FFT. This is a good simulation of the surface wave spectra shown in Fig. 1. However, skywave propagation generally imposes a line broadening of these Bragg lines due to ionospheric turbulence and multipath propagation. To simulate this behavior, we modeled the Bragg lines by narrowband Gaussian processes as well, with line widths narrower than those of the second-order structure. This was accomplished in the following manner.

First, a real-time series was generated consisting of Gaussian white-noise samples. This was done by using a random number generator function from the DEC VAX VMS library and by summing 20 of these random values between 0 and 1 to create a single noise sample with a value between 0 and 20. There were 1024 of such sums created. According to the Central Limit Theorem, a series of samples, each consisting of such a sum of values from any distribution, will approach a Gaussian distribution, and 12 samples is a typical working number to use in such a sum (see, for example, Burington and May [4, p. 195]). Hence, 1024 of such sums, each consisting of 20 random values, constitutes a white Gaussian distribution, irrespective of what function the random number generator represented. Figure 2 shows one such time series of 1024 noise samples.
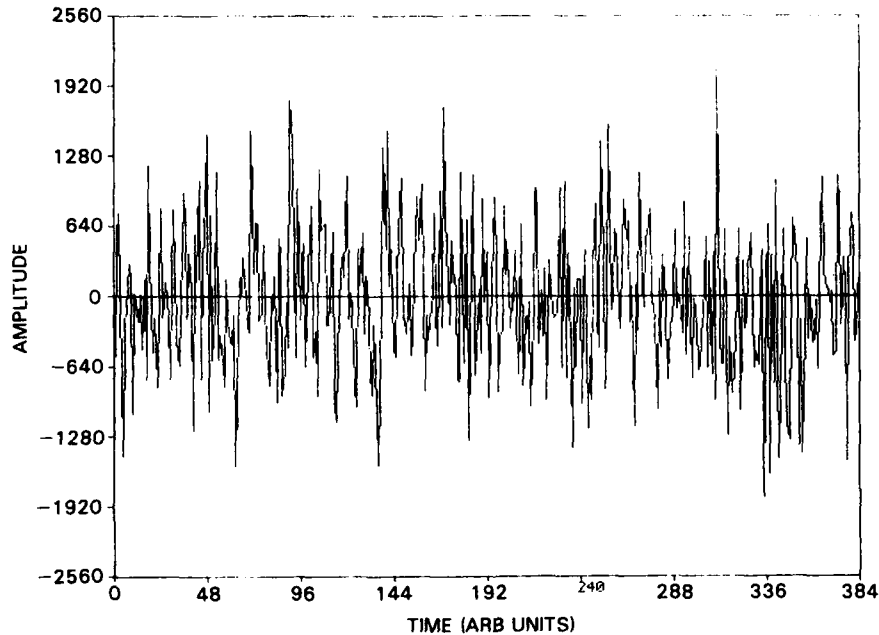
Fig. 2 — An example of 256 points of simulated white noise is shown, generated by a random function generator. These were used as the starting point for the simulated clutter contributions described in the text.

This time series of 1024 real points was then Fourier transformed to produce a complex spectrum, with 1025 real and 1025 imaginary points, $A(J) + iB(J)$, $J = 1$ to 1025. Because the time series input to the Fourier transform was real, the complex output is complex-conjugate symmetric about the midpoint, No. 513. That is, the real part of the Fourier transform is symmetric about the midpoint: $A(1026 - J) = A(J)$; whereas the imaginary part is symmetric in magnitude, but opposite in sign: $B(1026 - J) = -B(J)$. The power spectrum created from this transform is then symmetric about the midpoint.

This complex Fourier transform was then multiplied by a digital filter function, $D(J)$, which was also symmetric about the midpoint. This symmetry in the filter function was desirable to maintain a real-time series output when the resultant symmetric product series was inverse-Fourier transformed. This real-time series was desirable because of the limitation to real input data imposed by the variety of spectral estimation algorithms available in the Inter Laboratory Series (ILS) commercial digital-processing software package. This is not really a limitation, since complex data can be transformed to real data with twice the sample rate and processed without any loss of information. This was done with

4

the field data to be discussed in the next report of this series. The digital filter function used was that of a Gaussian profile, given by:

$$F(J) = \exp\{-([J - (PKHZ/5.)*256]/NDOPWID)^2\} \tag{4}$$

where *PKHZ* is the frequency of the desired peak in the spectrum in hertz, and *NDOPWID* is an integer defining the width of the filter. Figure 3 shows the complex frequency spectrum that is derived from the product of the Fourier transform and this filter function, for a value of *NDOPWID* = 4. Figure 4 shows the inverse-Fourier transform real-time series. Assuming a 10 Hz pulse-repetition-frequency (PRF), the ambiguous and symmetric power spectrum is also 10 Hz wide, 5 Hz of which is unambiguous.
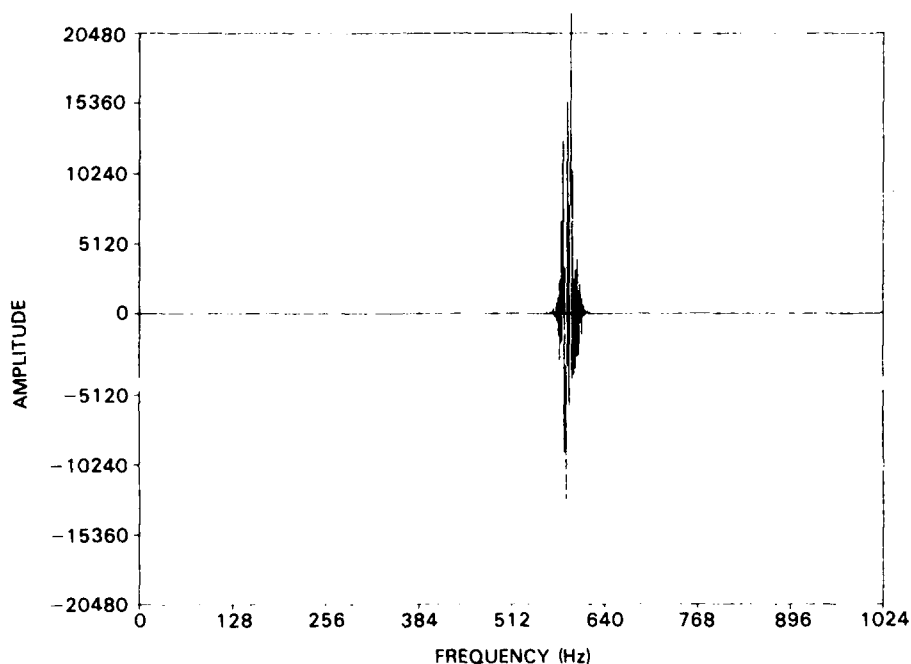
Fig. 3 — The Fourier transform of the real part of the noise of Fig. 2, after being multiplied by a narrowband filter function in the frequency domain. The filter width was adjusted to simulate the first-order Bragg lines and the second-order clutter contributions with other independent time series.

For the first method, as mentioned earlier, sinusoids were used to represent the first-order Bragg lines, one a 2.1 Hz sine wave, the other a 2.9 Hz cosine wave. Based on zero true Doppler centered at 2.5 Hz in the spectrum, these Bragg line shifts of 0.4 Hz represent a radar frequency of roughly 15 MHz. For the second method, in which the above filtering technique of a white-noise process was used to represent the Bragg lines, a value of *NDOPWID* = 2 was used for these components. The filter used to generate the two Bragg lines was centered at 2.1 and 2.9 Hz.

Similar processes were executed to construct the second-order broader band Doppler contributions lying between the Bragg lines and to either side. For the second-order contribution centered about zero Doppler, the value for *NDOPWID* = 16 was used. For the structure on either side of the two Bragg lines, *NDOPWID* = 8 was used. A sixth time series of very low-level white noise was generated by using the same technique described above, but without filtering, to represent the noise floor.
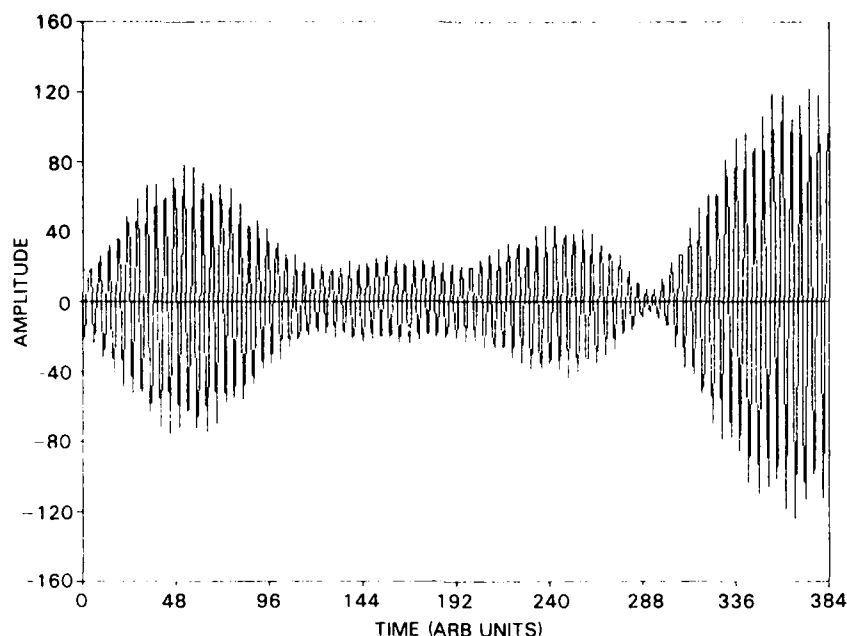
Fig. 4 — A portion of the time series generated by inverse-transforming Fig. 3 back to the time domain. This was added to other similar time series to represent a composite clutter time series as described in the text.

The Jth sample of each of the six time series was then simply summed point by point across the series of 1024. However, an appropriate amplitude scaling factor was used for each, so that the Fourier transform of the resultant time series simulated a realistic Doppler spectrum. Figure 5 is a power spectrum that shows the result for the method of using sinusoids for the Bragg lines. Figure 6 is a power spectrum that shows the result for the second method, using narrowband Gaussian processes to represent the Bragg lines. Figure 7 shows an example of more severe line-broadening of the first-order Bragg lines, in which a value of $NDOPWID = 4$ was used. And, finally, Fig. 8 shows a case in which the three second-order time series are 15 dB stronger than the last case. This case simulates a higher sea state condition than the last, in which the detection of a target in the region of the second-order structure would be more difficult.

SIMULATION OF TARGETS IN CLUTTER

To simulate targets in this clutter model, we simply used sinusoids of different amplitudes, stepping in 5 dB increments every 128 points, resulting in eight different amplitudes while scaling a 40 dB dynamic range in one 1024-point file. We also changed the Doppler shift relative to the Bragg lines from file to file to test the capabilities of the different processing algorithms in detecting the targets near the clutter. Figures 9 through 13 show examples for Doppler processing with 128 FFT input points (12.8 s coherent integration times (CITs)). for Doppler shifts from the center of the clutter spectrum of 3.5, 3.4, 3.3, 3.2, and 3.1 Hz, respectively. The last case has the target superimposed upon the second-order structure outside of the approach Bragg line. Hamming weighting was used for the FFT processing, but not for the spectral estimation analysis, since such weighting is known to produce line splitting in such estimates. In the following section, three different spectral estimation techniques are compared to determine a best estimator, and then the effects of processing parameter variation are studied for optimizing the quality of the spectral estimation.

Fig. 5 — A simulated clutter spectrum in which the first-order Bragg lines are represented by a sine and cosine function; the second-order contributions are represented by narrowband filtered white-noise time series as in Fig. 4. This figure is representative of surface-wave HF sea scatter with no ocean surface currents present.
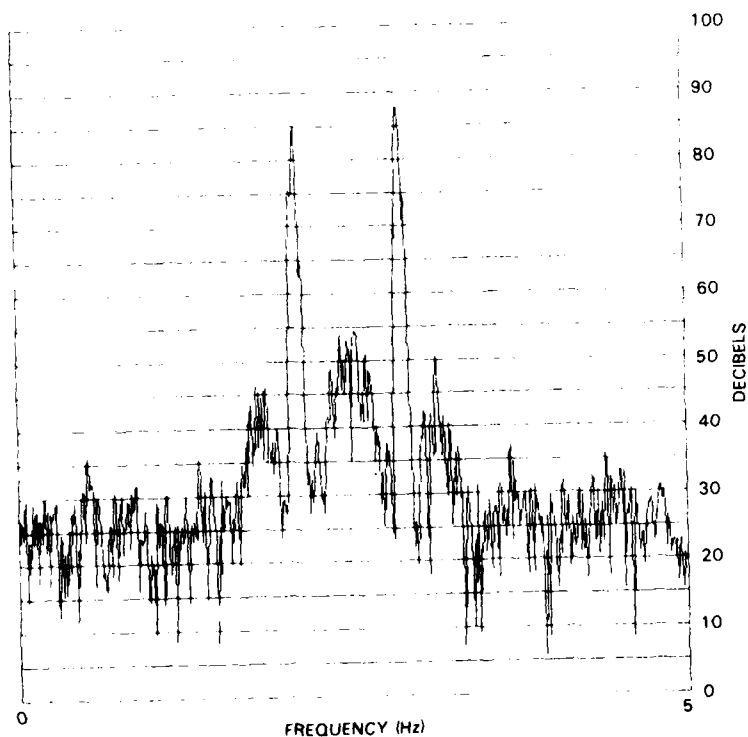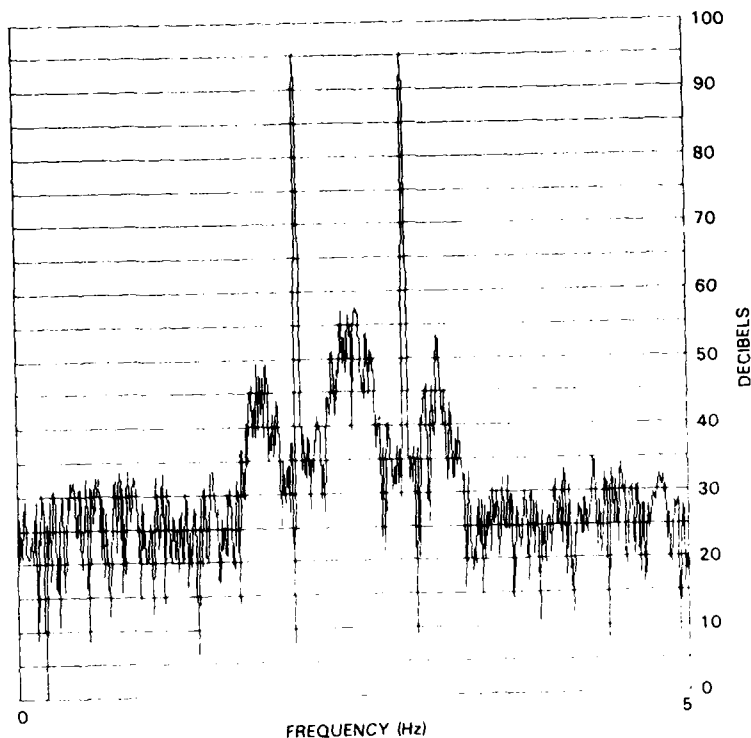

Fig. 6 — A simulated clutter spectrum in which the first-order Bragg lines are represented by very narrowband-filtered noise; second-order contributions are represented by the same narrowband-filtered white noise of Fig. 5. This figure simulates ionospheric broadening of the Bragg lines.

7
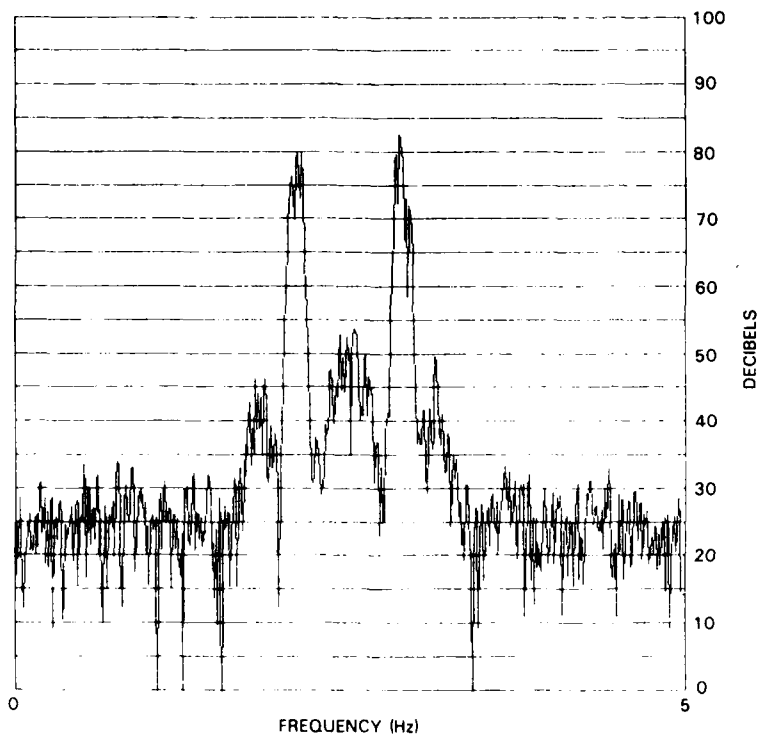
Fig. 7 — A simulated clutter spectrum in which the first-order Bragg lines are represented by a slightly broader filtered noise spectrum than was used in Fig. 6, simulating more severe ionospheric line broadening

Fig. 8 — A simulated clutter spectrum similar to Fig. 7, except that the second-order contributions are raised 10 dB relative to those in Fig. 7, simulating a higher sea state condition
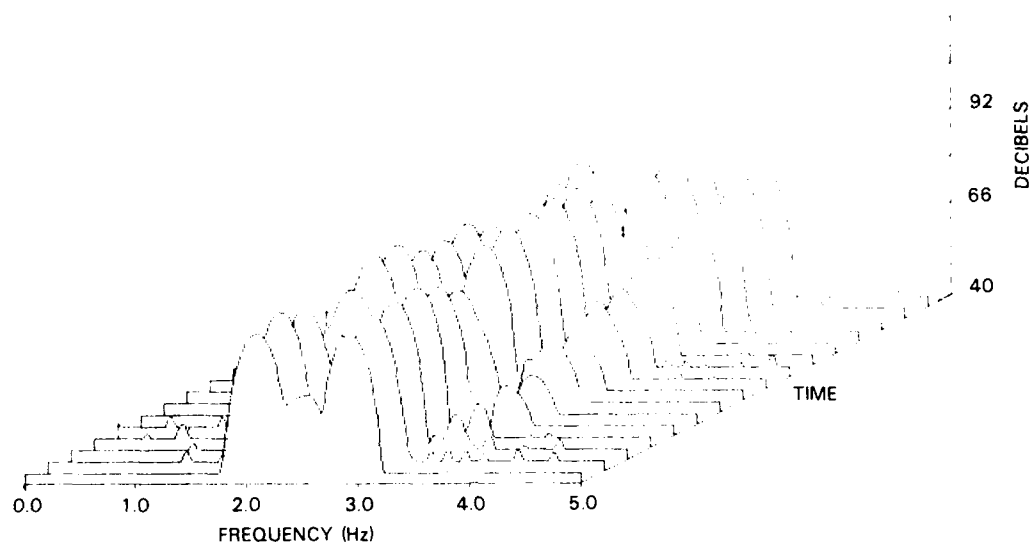

8
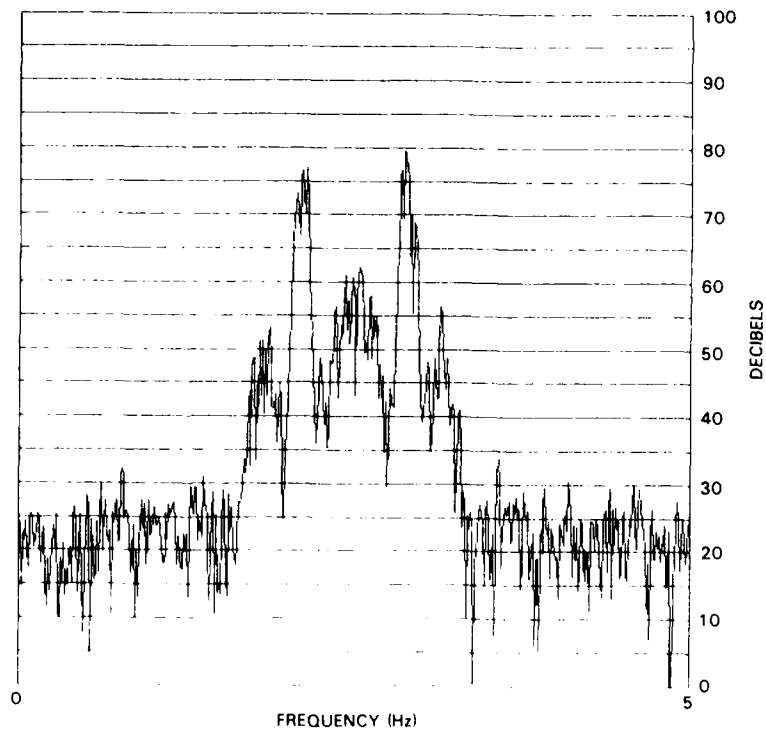
Fig. 9 — A target signal at 3.5 Hz Doppler added to the clutter time series used to produce Fig. 6. The target amplitude was raised by 5 dB each 128 points (12.8 s) to test the spectral estimation algorithms for varying clutter-to-signal ratios. The FFT spectrum shown here was produced with a 6.4-s integration time (64 points), but with zero filling with an FFT operating on 256 points.
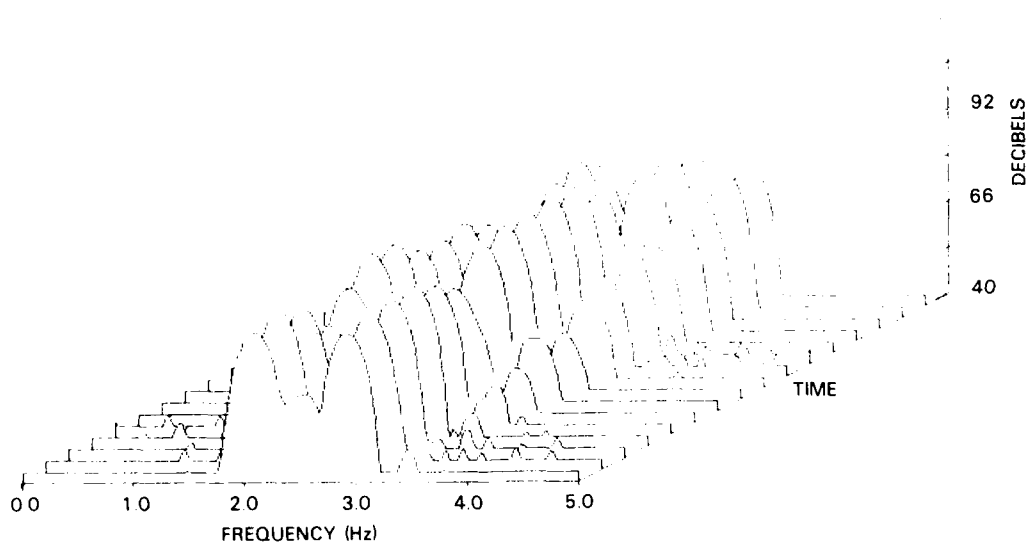
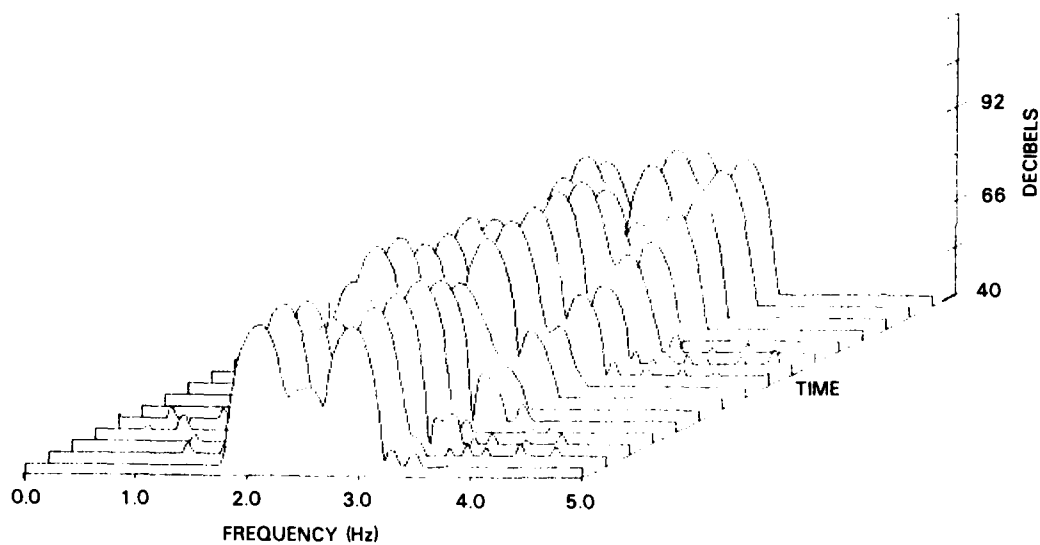Fig. 10 — This figure is similar to Fig. 9, but with a 3.3 Hz target Doppler shift

Fig. 11 — This figure is similar to Fig. 10, but with a 3.2 Hz target Doppler shift
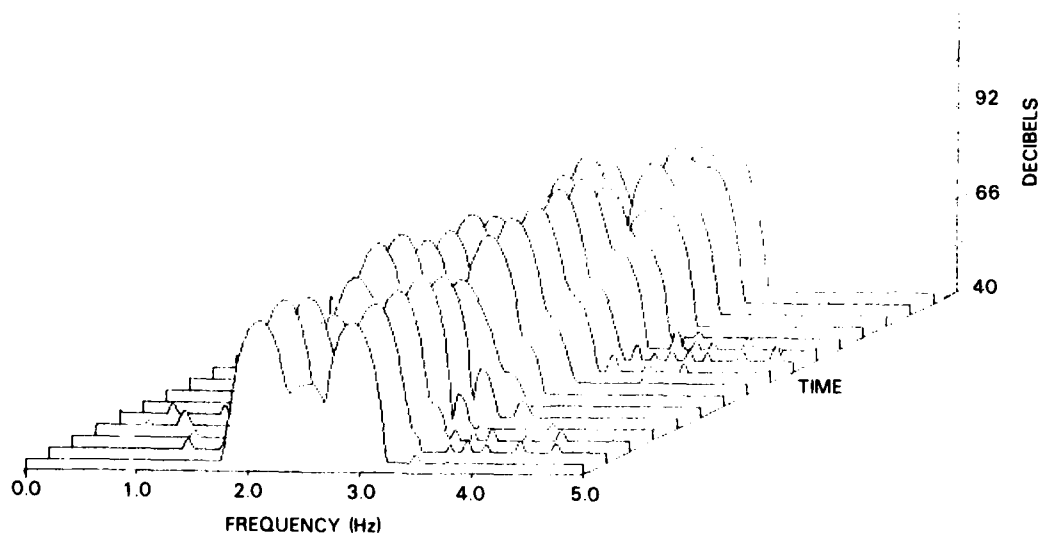
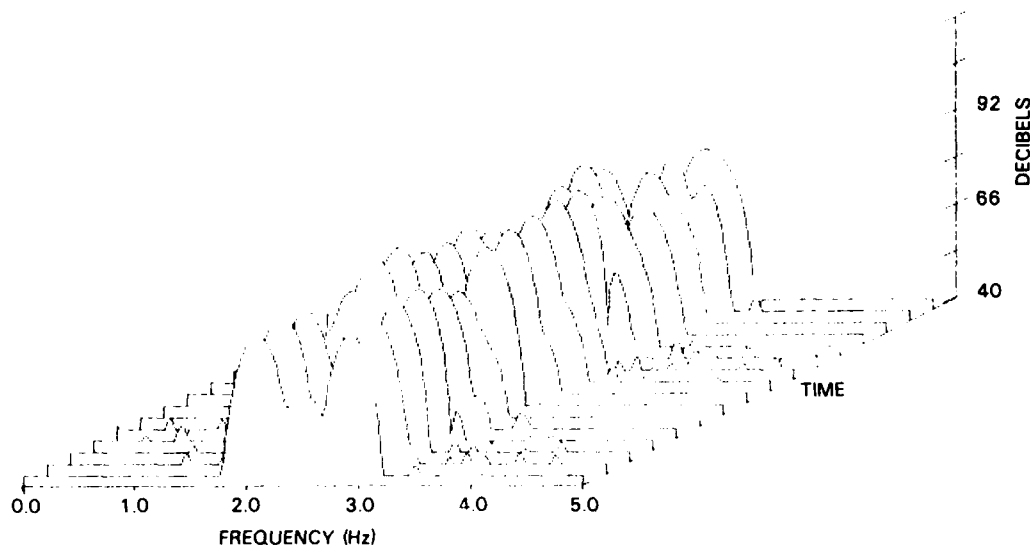Fig. 12 — This figure is similar to Fig. 11, but with a 3.1 Hz target Doppler shift

Fig. 13 — This figure is similar to Fig. 12, but with a 3.0 Hz target Doppler shift

COMPARISON OF SPECTRAL ESTIMATION ALGORITHMS ON SIMULATED DATA

Three different spectral estimation algorithms were tested on these data for several values of the analysis parameters, and one was chosen for further testing since it appeared to be superior to the other two. The estimators were (a) the maximum entropy method (MEM) of Burg, including his modified method; (b) a covariance matrix inversion method; and (c) an autocorrelation method. The second two methods are discussed in detail in Markel and Grey [5], while the Burg algorithms are to be found in the IEEE reprint series publication, "Modern Spectral Analysis" edited by Childer [6]. The effects of time-weighting the data are found to be different for the three different techniques, and these results are also presented in the following paragraphs.

Figure 14(a) shows the results of processing the data of Fig. 9 with the three spectral estimators for an order of 6 for the Burg, covariance, and autocorrelation methods running top to bottom. Hamming weighting was applied for this case, and using 64 input data points for each estimate (6.4-s CIT). The choice of a given even order will fit one-half that number of peaks in the unambiguous Doppler domain of radar $PRF/2$. (The other three poles will locate the symmetric peaks in the ambiguous half of Doppler space.) The results of the Burg and covariance method are identical, and they are very similar to the autocorrelation result except for the minor peak found between the Bragg peaks by the first two methods, presumably representing the second-order radar scatter in this region.

Figure 14(b) shows the same analysis but without any time-weighting of the data, and the differences are striking. The Burg method shows narrower peaks on the first-order Bragg lines and an enhanced ability to detect the target, which now appears strongly in the last four spectral estimates and weakly in two of them. The covariance method is able to calculate an estimate for only three of the time periods, probably due to the inability to evaluate the covariance matrix for this case. The autocorrelation method yields broader peaks than for the unweighted case and is unable to detect the target in any of the estimates.
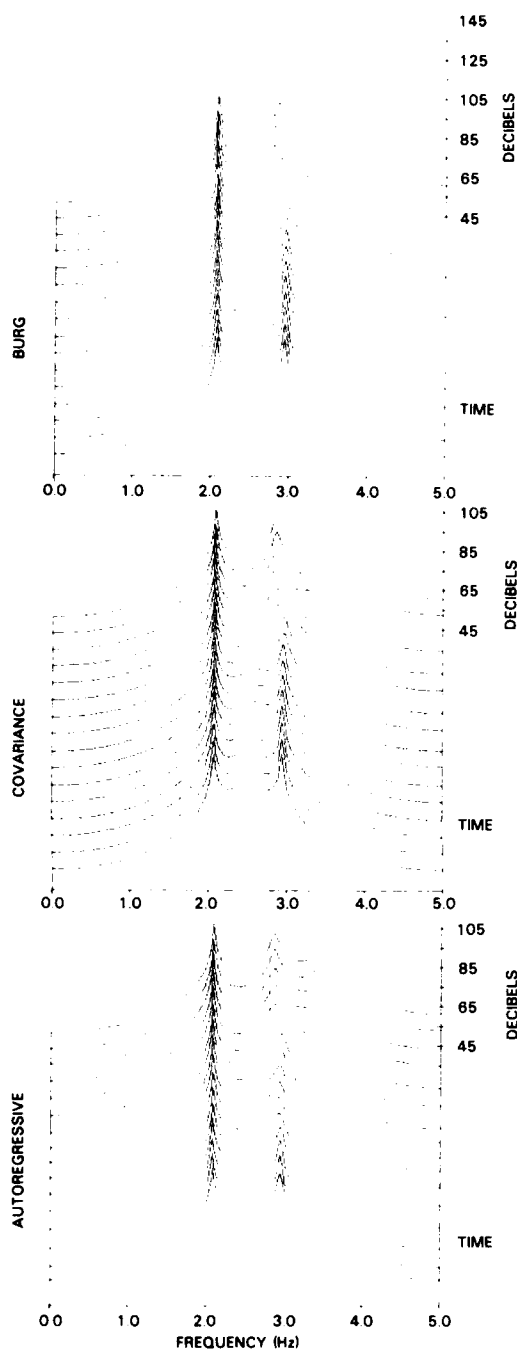
Fig. 14(a) — The results of three different spectral estimation algorithms are applied to the data of Fig. 9, by using a six-pole model in each of the Burg MEM, a covariance method, and an autocorrelation method for a 6.4-s integration period. Hamming time weighting was applied before the estimates were calculated.
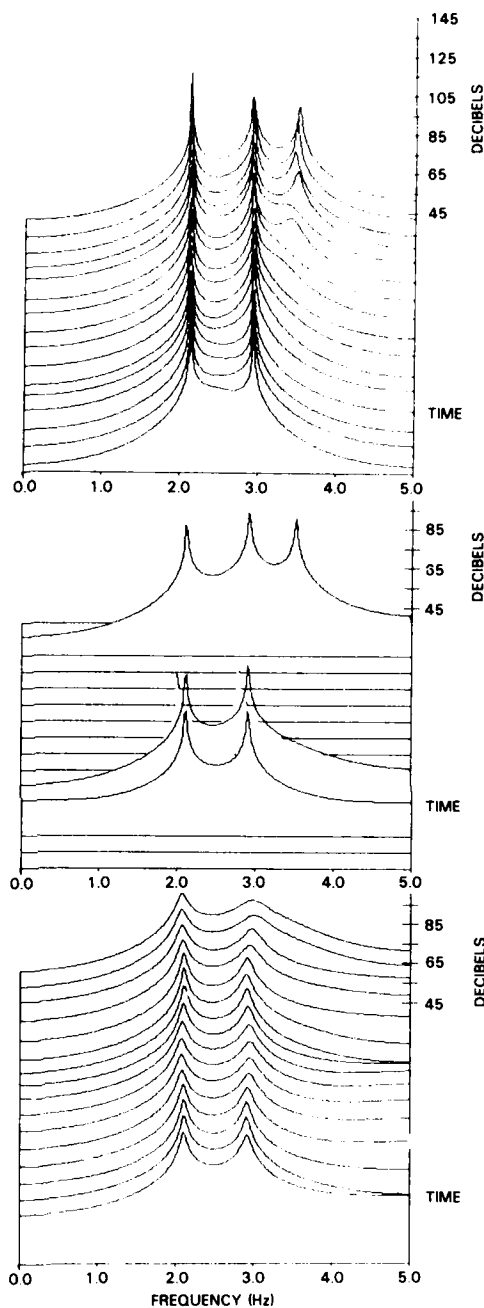
Fig. 14(b) — An analysis identical to that of Fig. 14(a), but with no time weighting

Figure 15(a) shows a time-weighted comparison of the three techniques for an order of 12, with the Doppler frequencies of six peaks estimated. Again, the Burg and covariance method yield virtually identical results. The autocorrelation method yields a broader peak for the target return than do the other two for the top six traces. The seventh and eighth traces from the top no longer define any peak for the target for the autocorrelation method, whereas a slight shoulder is still present for the other two techniques. This weak return is marginally useful for field data applications, such as a corroboration of a better defined peak as in the first few traces for the top in a time-series of spectra of this type. Hence, qualitatively, the first two techniques are to be considered as producing somewhat better results than the third for our application. Note the splitting of peaks which occurs for many of the spectra, a result of forcing two peaks to the largest amplitude returns in the spectra. Eliminating time-weighting for the 12-pole models, shown in Fig. 15(b), yields results similar to the sixth-order case: enhanced detectability for the MEM, failure to calculate several spectra for the covariance method, and a poorer detection capability for the autocorrelation method.

In Fig. 16(a), increasing the order to 18 begins to show differences between the Burg and covariance methods, in a sharpening of some of the peaks in the first few spectra from the bottom, but the results are still very similar. Each of these two is superior again to the autocorrelation method for identifying the target return for increasing clutter-to-target ratios. Results for no time-weighting are again similar to those for the previous models and are shown in Fig. 16(b).

Finally, Fig. 17(a) shows a more definitive difference between the three techniques for the time-weighted case, for an order of 24. The covariance model simply does not produce estimates for some CITs, presumably due to the inability to calculate the covariance matrix again. In the first spectrum, it does give a better estimate of the target return. The unweighted case again shows results similar to the previous cases: difficulty in calculating with the covariance method, poorer performance for the autocorrelation method, and improved performance for the Burg method. It is apparent that the Burg method is superior to the other two techniques and does better for unweighted data than weighted. The 24-pole case was also applied using the same three models, but for data in which the first-order Bragg lines were represented by very narrowband filtered noise instead of sinusoids. These results are shown in Fig. 18 for the cases of Hamming weighting and no weighting. Although the target levels have risen relative to the clutter peaks, the detectability of the target is only moderately improved.

A comment can also be made here regarding the order of the method chosen to represent a process. For modeling a process by use of spectral estimation techniques, it is typically suggested that the order of the model be twice the number of spectral peaks expected. However, because only a single pole is devoted to each spectral contribution, the skirts of the single pole can sometimes prevent a weaker signal from being identified, particularly with increasing noise levels. In overspecifying the model, one allows narrower skirts on a large signal at the expense of inviting the line-splitting effect on the peak. Thus, two or more spectral peaks are associated with the first-order Bragg lines as a result, but allow a much narrower spectral feature for the Bragg clutter line. Since the Bragg lines may be split in any case, as we have simulated in Figs. 6, 7, and 8, due to amplitude modulation by signal fading, this is not necessarily a poor representation of the spectrum in this case. If one were attempting to accurately locate the position of the Bragg peak, for ocean surface-current mapping for example [7], one would probably choose an order of four. However, the present interest is one of locating a weak target return in the presence of a much larger clutter line, at the expense of an accurate representation of the spectral content of the clutter. Thus, overspecifying the model order appears to work to an advantage for this application.
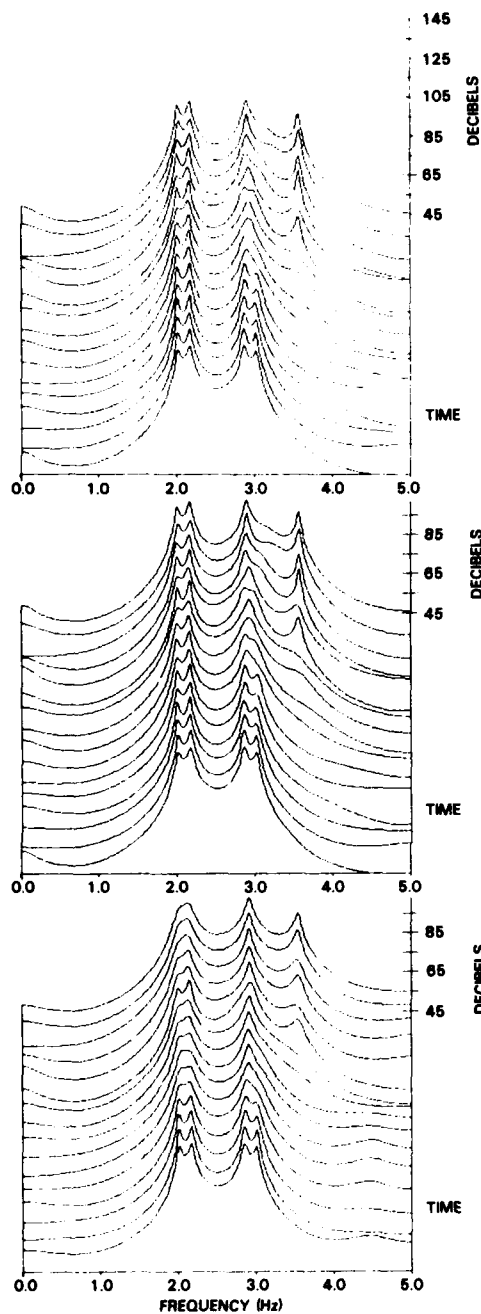
Fig. 15(a) — The same algorithms are applied
to the data of Fig. 14, but by using a 12-pole
model and Hamming weighting. The Burg and
covariance methods produce identical results
now, and yield four lower amplitude peaks not
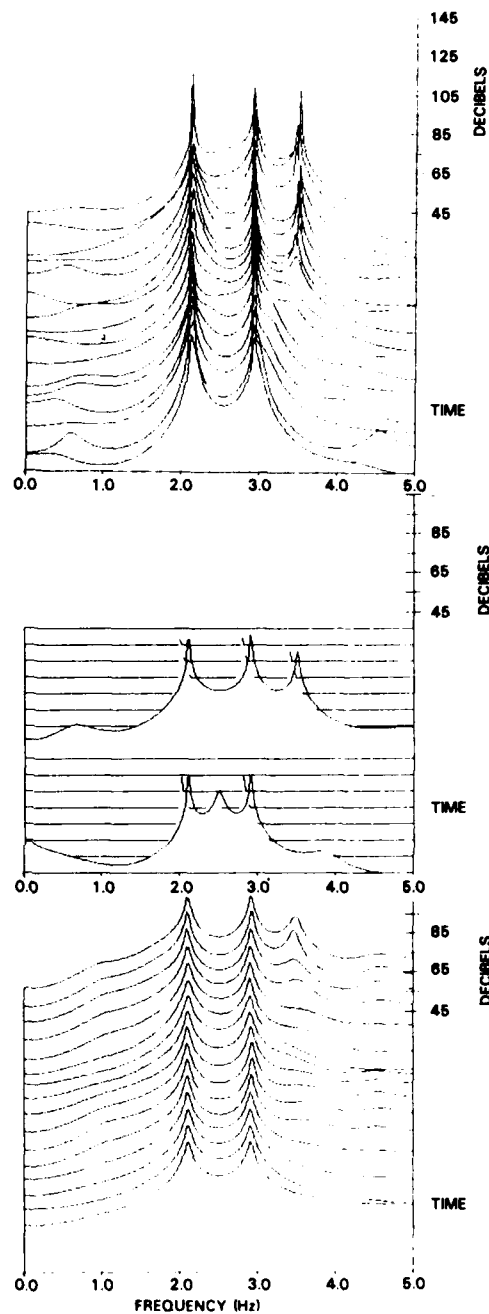seen in the six-pole model.

Fig. 15(b) — An analysis identical to that
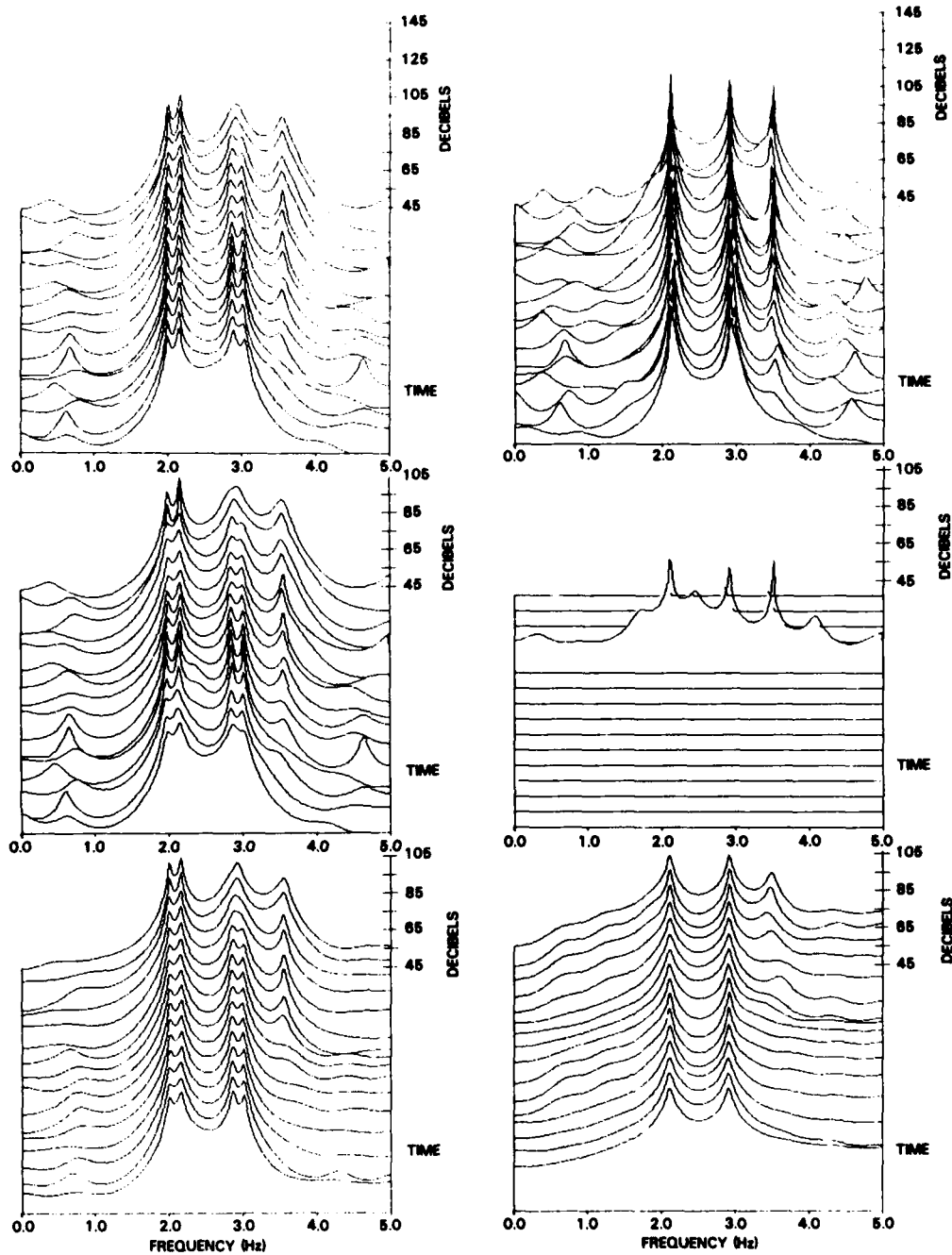of Fig. 15(a), but with no time weighting

Fig. 16(a) — The same algorithms are applied to the data of Fig. 14, but by using an 18-pole model and time weighting. The Burg and covariance methods show some differences now, show better detection capability than the 12-pole model, and are far superior to the auto-correlation model.

Fig. 16(b) — An analysis identical to that of Fig. 16(a), but with no time weighting
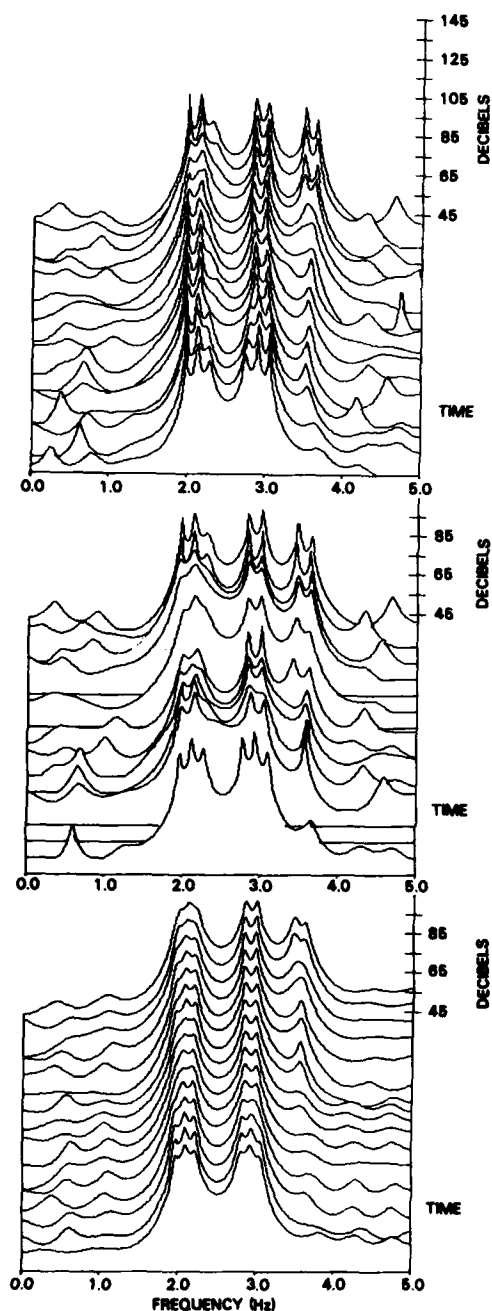
15

Fig. 17(a) — The same algorithms are applied to the data of Fig. 14, but by using a 24-pole model and time weighting. The Burg and covariance methods show even greater differences now, with the covariance model unable to produce spectral estimates in 4 of the 16 time periods.
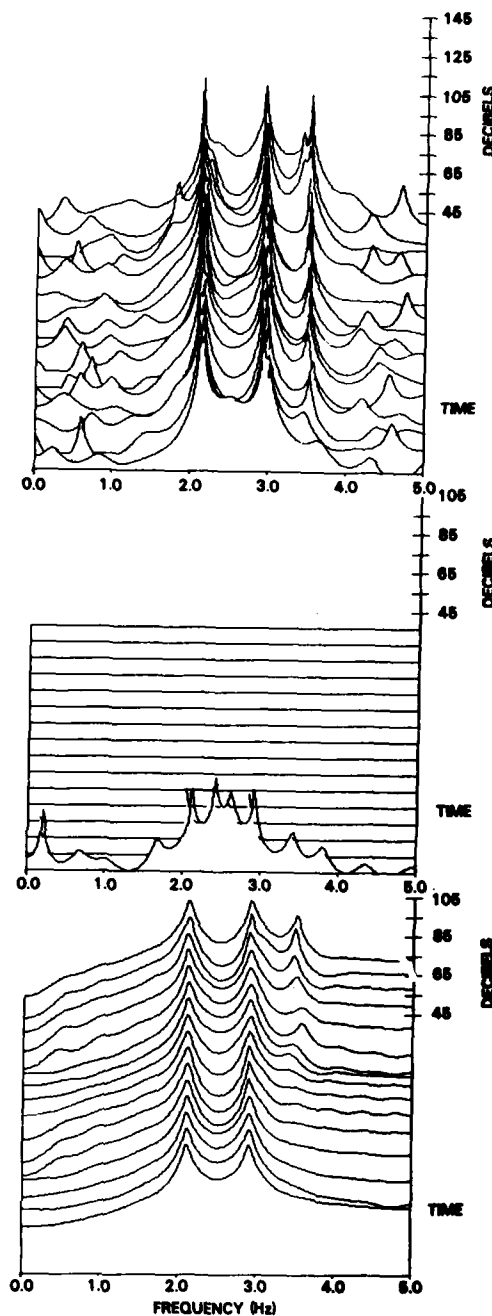
Fig. 17(b) — An analysis identical to that of Fig. 17(a), but with no time weighting
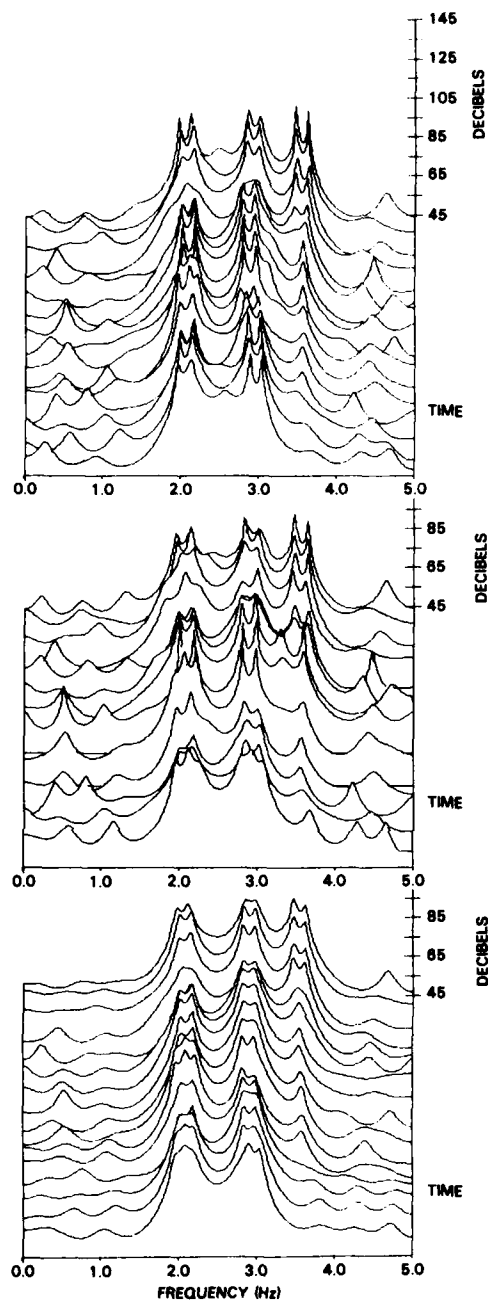
Fig. 18(a) — A 24-pole model is applied now to the data of Fig. 6, in which the Bragg lines are narrowband filtered noise instead of sinusoids, and so are slightly broadened compared to the previous figures. All of the methods show an improved ability to detect the target relative to the clutter, indicating the peak clutter-to-signal ratio is the primary influence and not the total energy in the Bragg line.
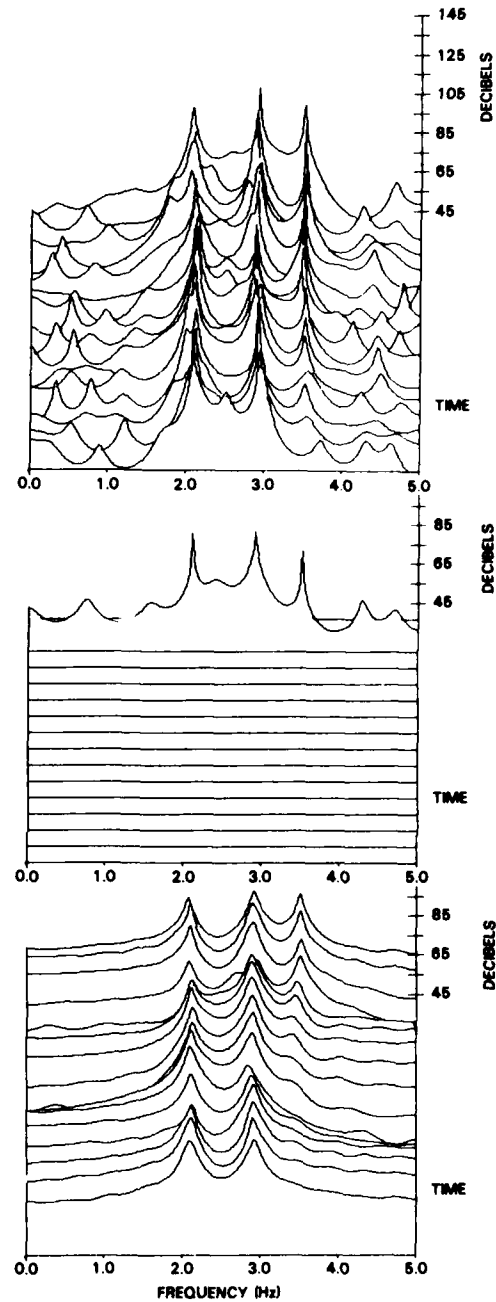
Fig. 18(b) — An analysis identical to that of Fig. 18(a), but with no time weighting

LIMITS OF TARGET TRACKING WITH TARGET-CLUTTER COALESCENCE

In this section we consider the optimum order for tracking a target of varying amplitude for a given figure, with the target progressively approaching the clutter in Doppler from one figure to the next. We consider the Burg method in all cases, with no time-weighting. Figure 19 shows a comparison of orders 18, 24, and 29 (maximum available from the ILS processing package) for a Doppler frequency of 3.5 Hz. The approach Bragg line was centered at 2.9 Hz, and the second-order continuum contribution was centered at 3.173 Hz. It is apparent that the highest order model allows the best target detection capability for this Doppler shift. The same holds true for target Doppler shifts of 3.3, 3.2, 3.1, and 3.0 Hz, in Figs. 20 through 23. Progressively fewer target identifications are made as the target coalesces with the clutter. As a comparison, Fig. 24 shows the results for the three orders and no target present, with the slanted display, and Fig. 25 shows the same information unslanted. Note that the 29-order case apparently picks up some of the second-order continuum in the sixth spectrum, which might be interpreted as a false alarm. However, this is the nature of nonstationary sea clutter, and such effects are to be expected, even with Fourier-transform processing.

It appears that the 0.3 Hz target Bragg-line separation of Fig. 21 provides the limiting case for target detection of one-half of the CITs showing a positive result for this clutter model. Two other spectra show a marginal peak that could be used as corroborative information in conjunction with the other positive identification.

ANALYSIS OF OTHER CLUTTER SIMULATIONS

As a final model comparison, we consider the other clutter models of Figs. 7 and 8 combined with the targets. These offer a more complex situation than Fig. 6, simulating ionospheric broadening of the first-order Bragg lines in the first case, and an added higher sea state condition as well for the second. Figure 26 shows, from top to bottom, the clutter simulations of Figs. 6, 7, and 8 with a target at 3.5 Hz. Figures 27 and 28 show the same clutter simulations with the target at 3.3 and 3.2 Hz, respectively.

A comparison of the top and middle plots of Fig. 26 shows that the broadening of the first-order Bragg lines actually makes the target more identifiable. It appears that the spectral estimator is more affected by the target-to-clutter ratio than by the width of the first-order Bragg lines. The target is visible in all of the spectra in the middle plot. By comparing the bottom plot with the middle one, it appears that the higher second-order structure outside of the Bragg line begins to affect the target detection for the same Bragg line width. One can conclude that the optimum environment for ship detection for this Doppler spacing is a moderate degree of Bragg line broadening due to the ionosphere with low to moderate sea states, which are responsible for the second-order scatter.

In Fig. 27 there appears to be very little difference in the ability to distinguish the target any better for one case than the other. There are between 10 and 12 positive appearances of the target in this case. Figure 28 shows a similar situation, with little difference between the detection capabilities. It appears that when the target return occurs in the region of the second-order clutter outside of the Bragg line, the detection probability is roughly 50% for the range of clutter-to-target ratios used here.
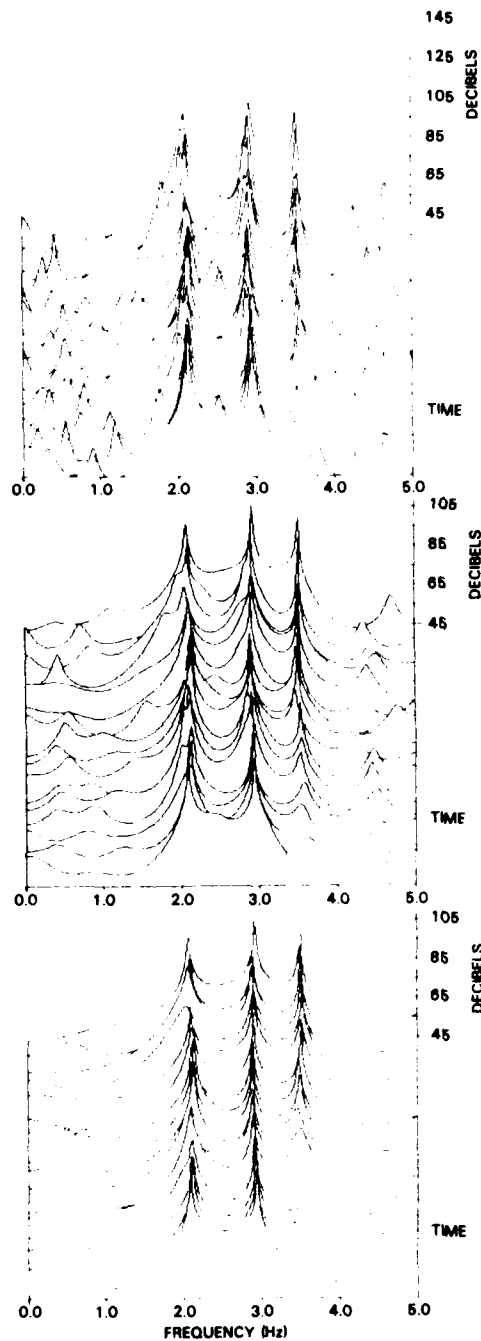
18

Fig. 19 — Three different pole models, 18, 24, and 29, are compared for the Burg model for a target Doppler of 3.5 Hz and no time weighting. There is only a slight improvement in going from 24 to 29 poles. A pole number of one half the number of input points is typically accepted as the maximum number before the model becomes overspecified.
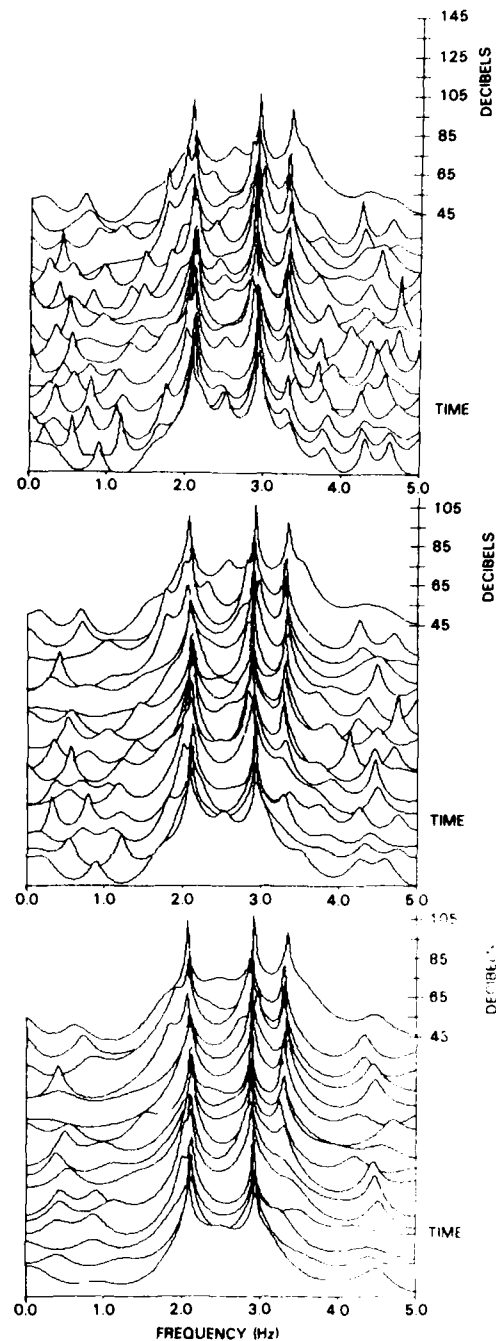
Fig. 20 — The same three models of Fig. 19 are used with a target Doppler of 3.4 Hz. Now the last 9 spectra are detected with both the 24 and 29 pole models, in contrast to 14 or more spectra in Fig. 19, indicating the poorer detection capability the closer the target is to the Bragg line.
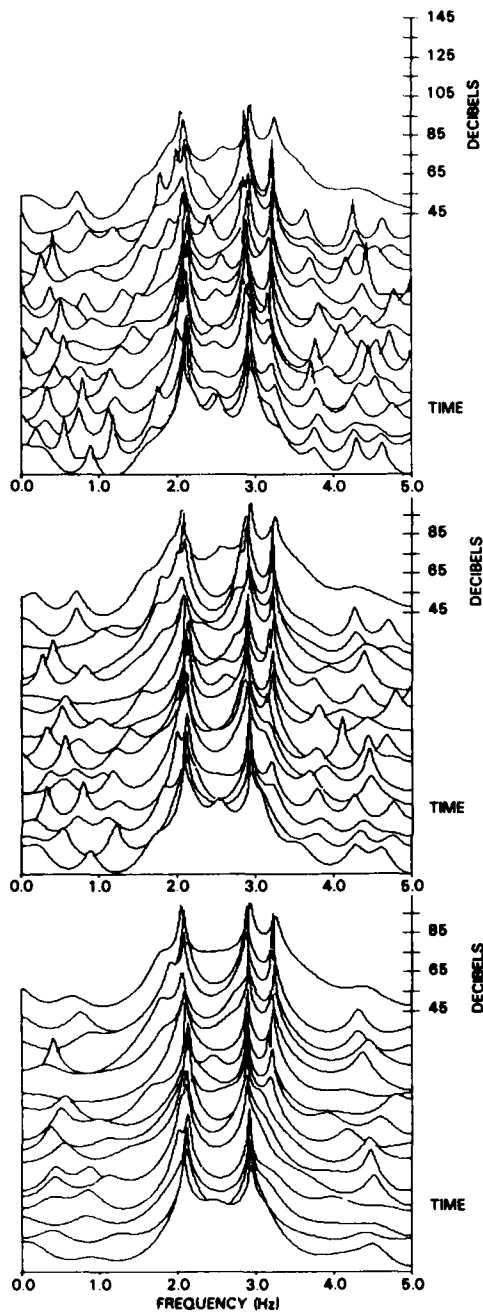
Fig. 21 — The same three models of Fig. 19 are used with a target Doppler of 3.3 Hz. The highest pole model offers improved detection capability in this case, allowing about half of the target returns to be detected.
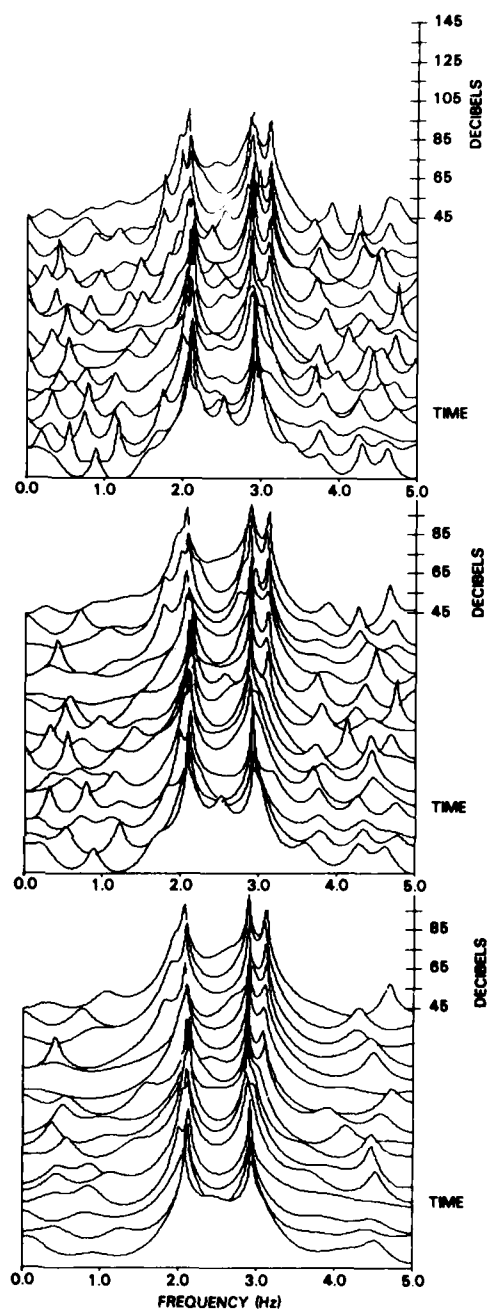
Fig. 22 — The same models used in Fig. 19 are used with a target Doppler of 3.2 Hz
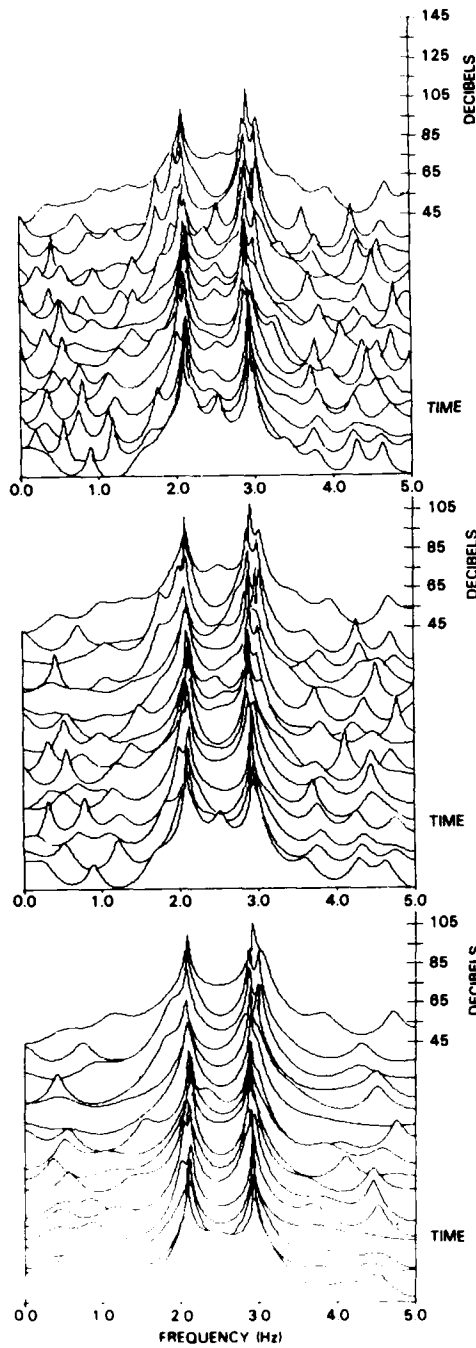
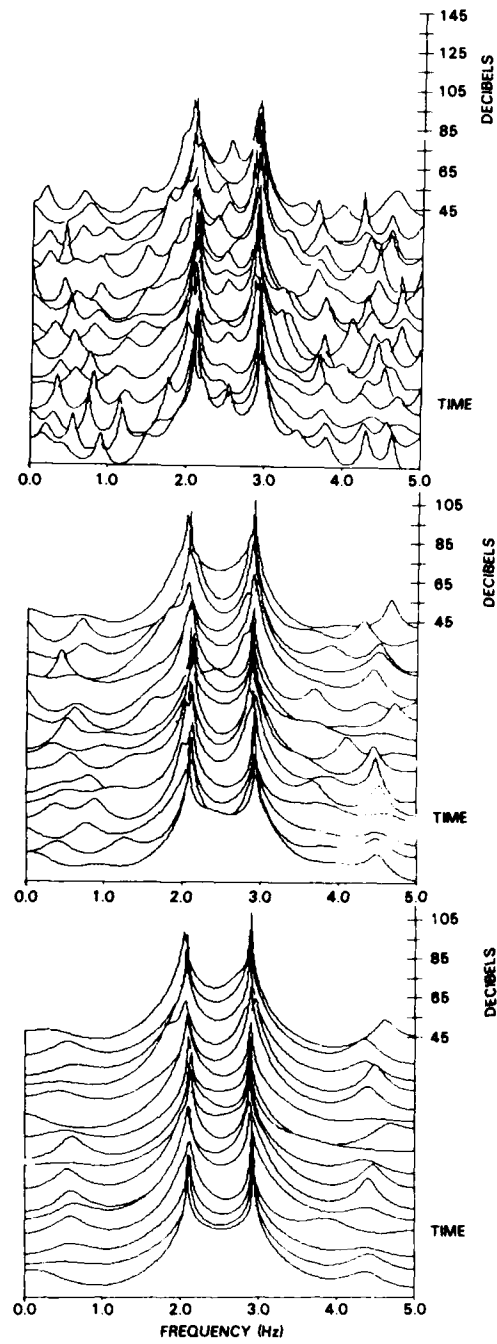Fig 23 — The same models used in Fig. 19 are used with a target Doppler of 3.1 Hz

Fig. 24 — The same models used in Fig. 19 are used without a target, to indicate the behavior of the clutter alone
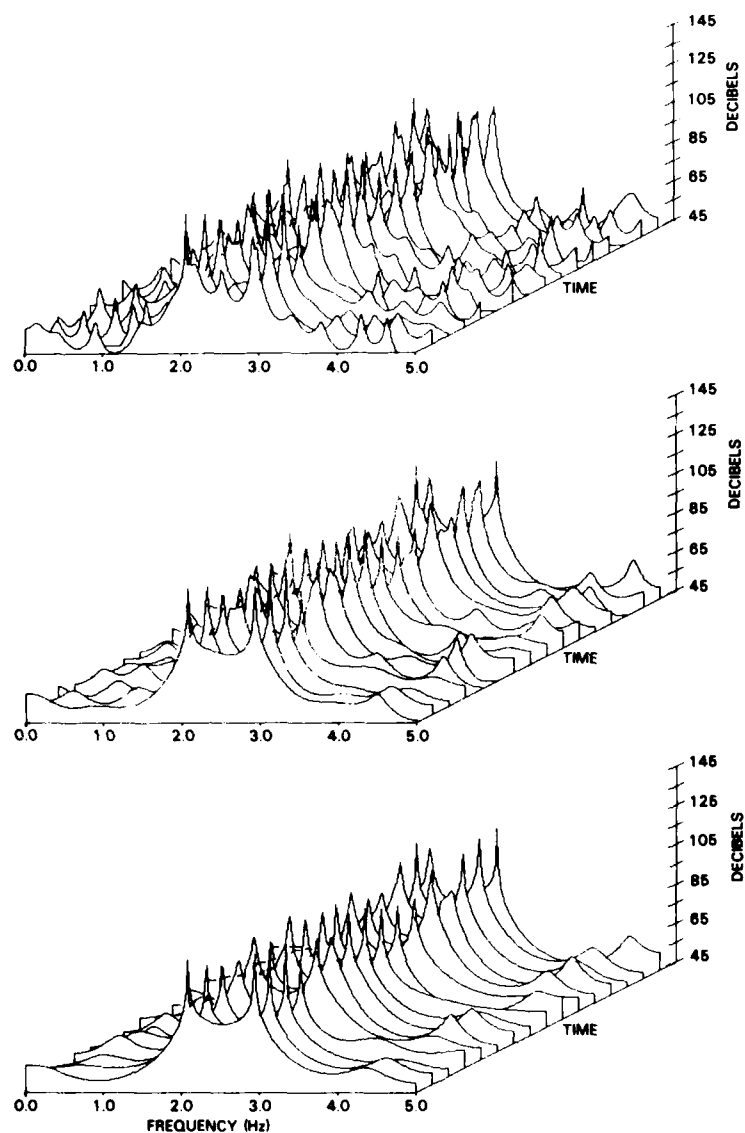
21

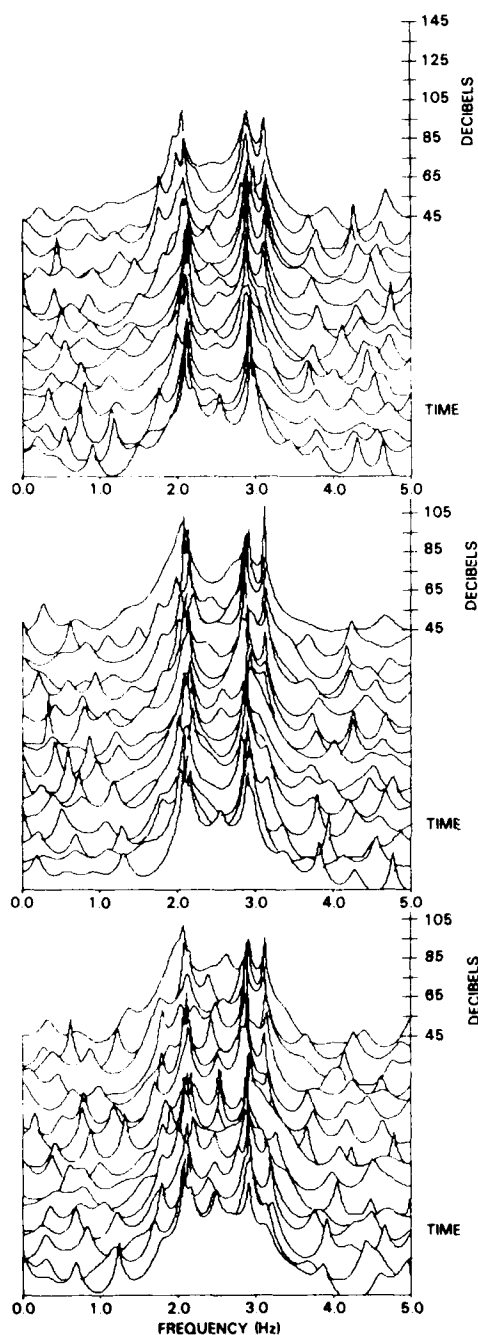Fig. 25 — The same results of Fig. 24, but with a canted display

Fig. 26 — The three different clutter models using the narrowband noise model for the Bragg lines of Figs. 6, 7, and 8 are shown with a target at 3.1 Hz. Broadening the Bragg lines allows the target to be seen more clearly for the same second-order clutter level. Raising the second-order clutter level in the bottom plot appears to produce a negative effect regarding target detection.
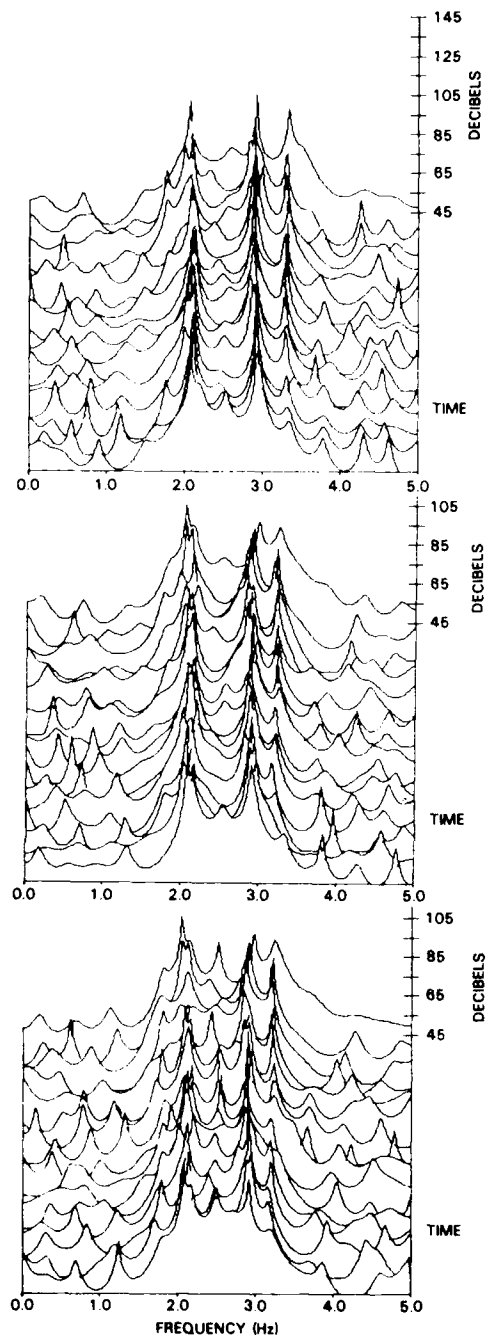
Fig. 27 — The same models used in Fig. 26 are used with a target Doppler of 3.2 Hz
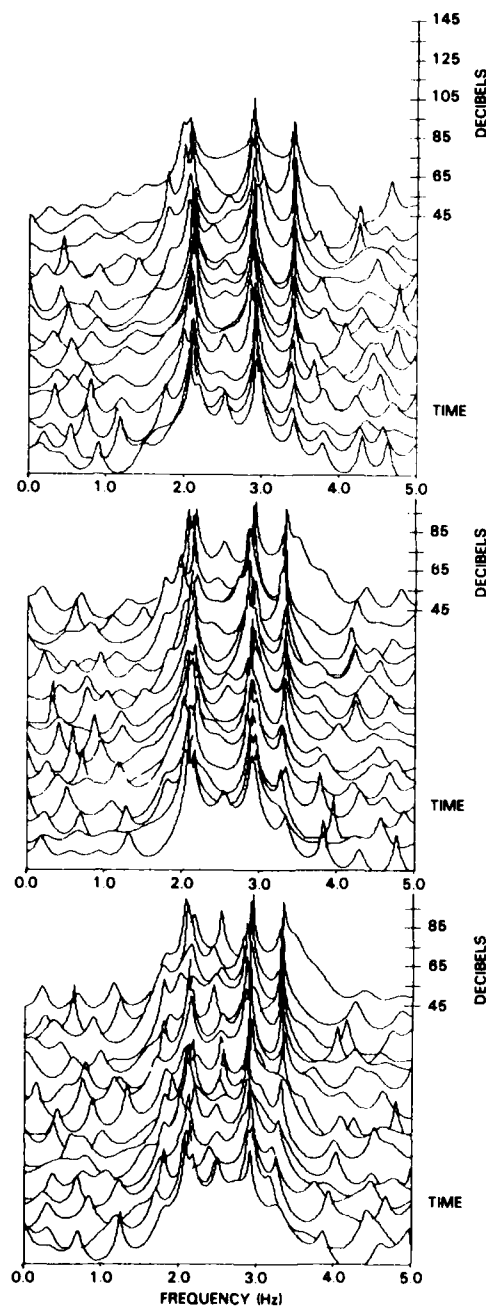
Fig. 28 — The same models used in Fig. 26 are used with a target Doppler of 3.3 Hz, essentially superimposed over the second-order clutter. This target-Bragg line spacing appears to present a limiting value for detection of the order of 50% here.

SUMMARY

In this report we have investigated the application of spectral estimation techniques to HF radar Doppler processing, with targets combined with clutter in simulated data. Several different models for the clutter were used. In all of these, the second-order clutter contributions were modeled by a white-noise spectrum operated on by a narrowband filter centered at the appropriate Doppler frequency. For the first type of model, the first-order Bragg lines were simulated by two sinusoids, producing very narrow line widths. For the other models, the Bragg lines were simulated by very narrow band-limited white noise to simulate line broadening by the ionosphere. Different combinations of Bragg line broadening and ratios of first- to second-order clutter levels were simulated. Targets were included as sinusoids with eight different amplitudes in a data file to study the effects of changing clutter-to-signal ratios by using different spectral estimation algorithms. Different target Doppler shifts were generated for individual files to study the effects of target-clutter coalescence, in each case combining with identical clutter data. This set of simulation models appears to provide a useful standard against which to compare other spectral estimation techniques in future work.

Three different spectral estimation algorithms were compared for several different conditions: the Burg maximum entropy method (MEM), the covariance method, and the autocorrelation method, as discussed in Markel and Grey [5]. The results showed improved target detectability as model order was increased from 6 to 12, to 18, and finally to 24 for the Burg and autocorrelation methods. The covariance model was unable to provide spectral estimates for higher order models, and the Burg model was judged as the best of the three. Improved target detectability was found for no time weighting of the data, in contrast to what one experiences in FFT processing.

As the target was allowed to approach the clutter in Doppler frequency, it was found that target detection becomes limited for cases of Doppler differences of 0.2 Hz between the target and the Bragg line. For this case, only 50% of the spectra produced target detectability for the range of target-to-clutter peak simulations studied. Such a range might be representative of a fading target return collected via an ionospheric skywave propagation mode.

As different models of the clutter were combined with the target and processed with the Burg algorithm for an order of 29, several interesting results appeared. First, as the Bragg line contributions were broadened for the same noise and second-order clutter levels, the target detectability actually improved. It appears that the important quantity in applying the spectral estimation algorithms is the ratio of the highest clutter amplitude to the target peak, rather than the total power contained in the Bragg line. This would imply that a moderate amount of ionospheric broadening actually improves the target detectability. Second, this held true as the second-order clutter level was increased for the same first-order line broadening just discussed, as long as the target was not superimposed on the second-order clutter. Finally, as the target was allowed to approach to within 0.2 Hz of the Bragg line, essentially lying on the second-order clutter, there appeared to be little difference between the three model orders used as far as target detection is concerned. All three models provided the same number of detections.

Further work in this area of HF Doppler simulation might be fruitful in several areas. Private discussions with John Shore, of NRL, indicate that application of his Cross Entropy Minimization technique might be very appropriate to this problem, serving essentially as a clutter cancellation technique. The technique depends on providing a first estimate as a clutter model, then comparing this with the data by including a target. As to actually employing such a technique on field data, such a comparison might be made of adjacent range bins, for example. Alternatively, a high spatial resolution range-azimuth cell could be compared with an average of several cells, effectively suppressing any targets present relative to the clutter. Moreover, the autoregressive moving-average (ARMA) models would appear on first principles to apply to this type of data, with its narrowband noise-like features, rather

than the AR techniques used here that model by using poles only. The simulated data set used here would appear to be a good standard against which to compare further.

REFERENCES

[1] W.F. Gabriel, "Spectral Analysis and Adaptive Array Superresolution Techniques," *Proc. IEEE* **68**, 654-666 (1980).

[2] D.W. Cooley, "Doppler Spectral Analysis of Ship-Echo Data Collected at the WARF: A Comparison of an Autoregressive Method to the Conventional FFT-Based Method," Technical Memo No. 1, SRI Project 7259, June 28, 1984.

[3] D.B. Trizna, "Estimation of the Sea Surface Radar Cross Section at HF from Second-Order Doppler Characteristics," NRL Report 8579, May 1982.

[4] R.S. Burington and D.C. May, *Handbook of Probability and Statistics with Tables*, 2nd ed. (New York, 1973).

[5] J.D. Markel and A.H. Grey, *Linear Prediction of Speech* (Springer-Verlag, New York. 1976).

[6] D.G. Childer, ed., *Modern Spectral Analysis* (IEEE Press, New York, 1976).

[7] D.B. Trizna, "Mapping Ocean Currents Using Over-the-Horizon Radar," *Int. J. Remote Sensing* **3**, 295-309 (1982).

DTIC

FILMED

4-86

END